FULL PAPER

Spectroscopic Evaluation of Mixing and Crystallinity of Fullerenes in Bulk Heterojunctions

Anne A. Y. Guilbert, Malte Schmidt, Annalisa Bruno, Jizhong Yao, Simon King, Sachetan M. Tuladhar, Thomas Kirchartz, M. Isabel Alonso, Alejandro R. Goñi, Natalie Stingelin, Saif A. Haque, Mariano Campoy-Quiles, and Jenny Nelson**

The microstructure of blend films of conjugated polymer and fullerene, especially the degree of mixing and crystallization, impacts the performance of organic photovoltaic devices considerably. Mixing and crystallization affect device performance in different ways. These phenomena are not easy to screen using traditional methods such as imaging. In this paper, the amorphous regiorandom poly(3-hexylthiophene) is blended with the potentially crystalline fullerene [6,6]-phenyl-C_{61}-butyric acid methyl ester PCBM and the amorphous bis-adduct. First, the degree of mixing of polymer: fullerene blends is evaluated using UV–Vis absorption, steady-state and ultra-fast photoluminescence spectroscopy. The blue-shift of the polymer emission and absorption onset are used in combination with the saturation of the polymer emission decay time upon fullerene addition in order to infer the onset of aggregation of the blends. Second, the crystallinity of the fullerene is probed using variable angle spectroscopic ellipsometry (VASE), electroluminescence and photoluminescence spectroscopy. It is shown that the red-shift of charge transfer emission in the case of PCBM based blends cannot be explained solely by a variation of optical dielectric constant as probed by VASE. A combination of optical spectroscopy techniques, therefore, allows to probe the degree of mixing and can also distinguish between aggregation and crystallization of fullerenes.

1. Introduction

The active layer of the best performing solution processable organic photovoltaic (OPV) devices is composed of a fullerene derivative blended with a conjugated polymer.[1] The microstructure of such blends is complex. It features a number of different phases that may include pure polymer, pure fullerene, an amorphous mixture of polymer and fullerene and, in the case of either component being crystalline, polymer or fullerene crystallites embedded within an amorphous material.

Polymer and fullerene are usually thermodynamically miscible over a certain range of composition, up to the thermodynamic miscibility limit that can be tens of wt% for PCBM in conjugated polymers.[2–6] Within this range of composition, mixing between polymer and fullerene takes place as a result of favorable interactions between the polymer and the fullerenes as well as the fast solidification rate when processing

Dr. A. A. Y. Guilbert, J. Yao, Dr. S. M. Tuladhar,
Prof. J. Nelson
Department of Physics and Centre for Plastic Electronics
Imperial College London
South Kensington Campus
London SW7 2AZ, UK
E-mail: jenny.nelson@imperial.ac.uk

Dr. M. Schmidt, Dr. M. I. Alonso, Prof. A. R. Goñi, Dr. M. Campoy-Quiles
Institut de Ciència de Materials de Barcelona (ICMAB-CSIC)
Campus de la UAB
Bellaterra 08193, Catalunya, Spain
E-mail: mcampoy@icmab.es

Dr. A. Bruno
ENEA – Italian National Agency for New Technologies
Energy and Sustainable Economic Development
Research Centre Portici – P.le E.
Fermi 1, 80055, Portici, (NA), Italy

DOI: 10.1002/adfm.201401626

Dr. A. Bruno, Dr. S. King, Dr. S. A. Haque
Department of Chemistry and Centre for Plastic Electronics
Imperial College London
South Kensington Campus
London SW7 2AZ, UK

Prof. T. Kirchartz
IEK5-Photovoltaik
Forschungszentrum Jülich
52425 Jülich, Germany

Prof. T. Kirchartz
Faculty of Engineering and CENIDE
University of Duisburg-Essen
Carl-Benz-Str. 199, 47057, Duisburg, Germany

Prof. A. R. Goñi
ICREA, Passeig Lluís Companys 23, Barcelona 08010, Spain

Prof. N. Stingelin
Centre for Plastic Electronics and Department of Materials
Royal School of Mines, Imperial College London
London SW7 2AZ, UK

from solution using deposition methods such as spin-coating. Demixing occurs at higher concentrations leading to the formation of fullerene clusters and polymer aggregates embedded in an amorphous polymer:fullerene phase. Furthermore, demixing can take place for as-spun films at concentrations lower than the thermodynamic miscibility limit due to more favorable interactions between one of the blend components and the solvent during film formation. In the following, we will refer to the concentration at which fullerene clustering happens as the onset of aggregation. Finally, demixing can be promoted by crystallization of one or both blend components. If the clusters do not exhibit long range order, we will refer to these clusters as aggregates, otherwise as crystallites. The organization of the fullerene moieties within the polymer matrix at both microscale and nanoscale influences OPV performance in different ways.

Microscopic phase separation, normally driven by a low miscibility of the fullerene and the polymer, has been reported to lead to poor charge generation and thus, to be detrimental to OPV performance. However, too high mixing is shown to be detrimental to the electron transport because of a lack of continuous pathway resulting in a high recombination rate.[7]

Crystallization within the segregated phases can be beneficial in several ways. Fullerene or polymer crystallization can increase charge carrier mobility. Fullerene crystallization is also believed to improve the charge separation process,[8–10] possibly through delocalization of the excited charge transfer state and polaron wavefunctions or through a reduction in Coulomb attraction due to increased local permittivity.

Both mixing and crystallinity/aggregation are, however, difficult to probe. Mixing can be quantified by small angle neutron scattering (SANS) on thick (~1 mm) as-spun blends,[2] by probing the interdiffusion of polymer and fullerene as a function of temperature in a bilayer architecture using dynamic secondary ion mass spectrometry (dSIMS)[3] or neutron reflectometry[4] or by probing the composition of the fullerene-rich phase by near edge X-Ray absorption fine structure (NEXAFS) spectroscopy on annealed blends that have reached thermodynamic equilibrium.[5] H^1 spin diffusion NMR has been shown to be a valuable method to probe phase separation.[6] Crystallinity of fullerenes is probed either by differential scanning calorimetry (DSC) on "bulk" samples or by grazing incidence wide angle X-Ray scattering (GIWAXS). All these measurements, whilst informative, are time consuming. Moreover they are usually performed on architectures that are very different from the as-spun thin films.

Optical spectroscopy such as UV–Vis absorption, steady-state[6,11–14] and time-resolved photoluminescence (PL)[15] spectroscopies and ellipsometry[16] have been also used to monitor phase separation in bulk heterojunction solar cells and to probe the crystallinity of the polymer. Optical spectroscopic techniques have the advantage to be non-destructive, quick and they can be performed directly on thin films. However, to our knowledge there are no reports of the use of optical spectroscopy to probe fullerene crystallinity in polymer:fullerene blends.

In this paper, we show, first, that we can use a combination of spectroscopic techniques to evaluate the degree of mixing of polymer: fullerene blends. Second, we demonstrate that spectroscopy can distinguish between aggregation and crystallization of fullerenes. We have selected an amorphous polymer, regiorandom poly(3-heylthiophene) (RRa-P3HT) blended with either the semi-crystalline fullerene derivative [6,6]-phenyl-C_{61}-butyric acid methyl ester (PCBM) or the amorphous bis-adduct (bis-PCBM) as model system.

We start by studying the mixing/demixing of PCBM blended with RRa-P3HT and of bis-PCBM blended with RRa-P3HT using UV–Vis absorption, steady-state and time-resolved photoluminescence (PL) spectroscopies in order to establish the apparent onset of aggregation. Then, we use complementary optical techniques to determine the crystallization of fullerenes in RRa-P3HT. These methods include variable angle spectroscopic ellipsometry (VASE) to probe changes in optical dielectric constant upon addition of fullerenes and PL and electroluminescence (EL) spectroscopy to study changes in the charge transfer (CT) emission. Finally, we demonstrate that PL and EL can be used efficiently to distinguish fullerene crystallites from aggregates.

2. Results

2.1. Mixing/Demixing of Fullerenes in RRa-P3HT

In this section, we use UV–Vis absorption spectroscopy and steady-state PL spectroscopy to infer the degree of mixing of the as-spun blends of RRa-P3HT:PCBM and bis-PCBM as it has been previously used to study the intermixed phase of PCBM blended with low and high molecular weight P3HT.[17] Then, we study the impact of mixing/demixing on the exciton lifetime.

Steady-state PL spectra of blends of RRa-P3HT:PCBM and RRa-P3HT:bis-PCBM of different polymer:fullerene ratios are plotted in **Figure 1**a,b. The peak around 2 eV (≈620 nm) is the emission peak of neat RRa-P3HT. Upon addition of fullerenes, the 0–0 emission peak of RRa-P3HT as determined by fitting the PL spectra (the fitting is explained in the method section and the PL spectra are shown in Figure S1 in Supporting Information) is blue-shifted (see Figure 1c) some 60 meV and more efficiently quenched. A peak at lower energies than 1.45 eV (> 850 nm) arises for few vol% of fullerene. This is assigned to the charge transfer state between the polymer and the fullerene. An additional peak centered around 1.7 eV (≈730 nm) arises for content of about 15 vol% of PCBM and about 20 vol% of bis-PCBM. The latter emission peak arises from the fullerene contribution and points towards the formation of pure fullerene domains. The polymer emission is strongly quenched upon fullerene addition up to about 5 vol% PCBM and 10 vol% bis-PCBM (see Figure 1d).

The polymer emission blue-shift can be explained by the strong intermixing of polymer and fullerene leading to conformational disorder in the polymer backbone, and hence to lower conjugation length.[18] If this hypothesis is correct, one should also observe the corresponding blue-shift in the absorption spectra of the polymer. The absorption spectra of blends of RRa-P3HT:PCBM and RRa-P3HT:bis-PCBM are plotted in Figure S3 in Supporting Information. The low energy absorption edge was determined by the intercept of the straight lines describing the low energy slope of the absorption and the low energy background signal. The resulting position of the absorption edge as

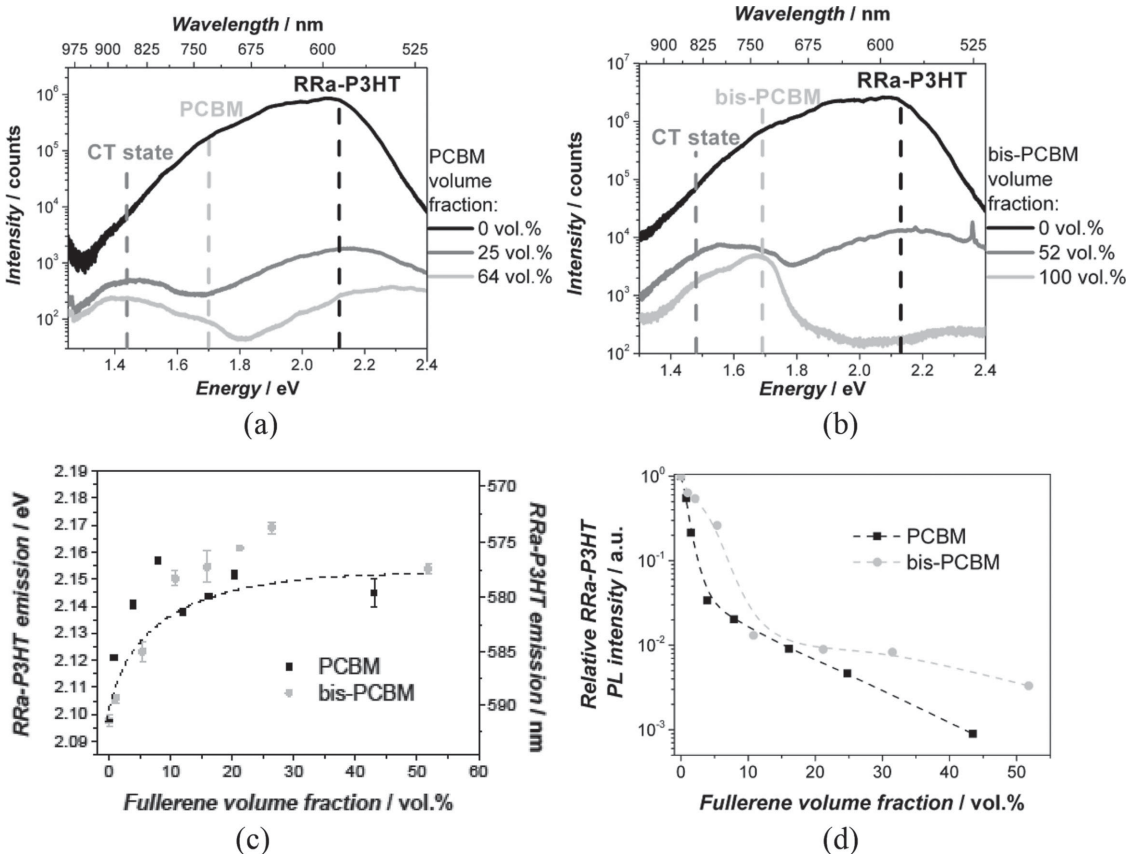

Figure 1. Photoluminescence spectra of a) RRa-P3HT:PCBM and b) RRa-P3HT:bis-PCBM blends. The excitation wavelength was 405 nm for RRa-P3HT:PCBM and 488 nm for RRa-P3HT:bis-PCBM. c) Energy of the 0–0 transition peak of RRa-P3HT emission as a function of fullerene content. The dashed line is a trend line. d) Relative RRa-P3HT emission intensity (the PL spectra are shown in Figure S2 in Supporting Information).

a function of fullerene concentration is plotted in **Figure 2**. The absorption edge shifts gradually to higher energies upon addition of fullerenes and starts to stabilize for fullerene loading higher than 25 vol% where the polymer emission peak also stabilizes. The total shift in absorption edge is about 60 meV (≈20 nm), in agreement with the shifts observed in the polymer PL. We conclude that the polymer emission blue-shift is indeed due to strong intermixing of polymer and fullerene. Thus, the stabilization of the polymer emission energy for fullerene contents of about 25 vol% points towards an onset of aggregation at those concentrations where the further addition of fullerene leads to no significant additional polymer chain disruption.

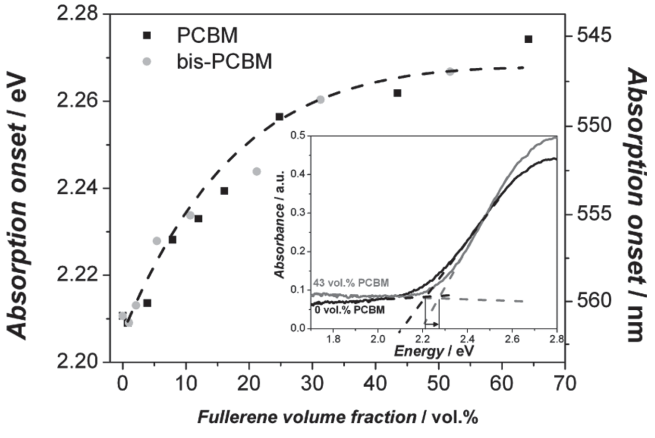

Figure 2. Absorption edge position of RRa-P3HT:PCBM and bis-PCBM (the absorption spectra are plotted in Figure S1 in Supporting Information). The absorption spectra of RRa-P3HT and RRa-P3HT:PCBM (43 vol%) showing the shift of the absorption edge and the way we have been determining its value is shown in the inset.

To further study the mixing/demixing of the fullerenes and RRa-P3HT, we use ultra-fast time resolved photoluminescence. Normalized ultra-fast time resolved emission decay traces are plotted for different fullerene loading in Figure S4 in Supporting Information. The excitation and detection wavelengths were 400 nm (≈3.1 eV) and 620 nm (≈2.0 eV) respectively, near the absorption and emission maximum of RRa-P3HT. The decays can be reasonably fitted by a mono-exponential kinetics within the time window of the experiment as it has been previously observed for amorphous conjugated polymers.[19–22] The resulting time decays are plotted as a function of fullerene content in **Figure 3**.

For both PCBM and bis-PCBM, the most substantial drop in polymer emission lifetime is observed upon addition of a few vol% of fullerene, up to around 10 vol%. For higher fullerene loading, the lifetime slowly decreases upon addition of PCBM while it saturates upon addition of bis-PCBM at a longer decay time than for PCBM.

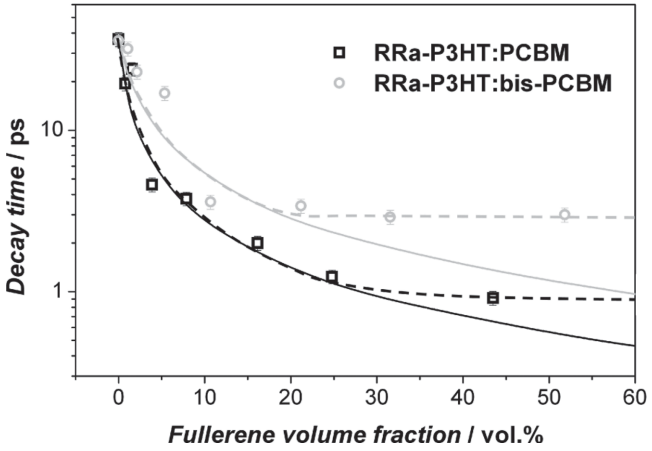

Figure 3. Decay times extracted from a single exponential fit of the time-resolved fluorescence decays of RRa-P3HT:PCBM and RRa-P3HT:bis-PCBM plotted in Figure S4 (Supporting Information). The solid line is calculated according to Equation 1. The dashed line is given for guidance.

To interpret the decay times we first consider the effect of composition on the PL decay time of a random solid solution of polymer and fullerene and fit the early drop in polymer emission lifetime using:[22]

$$\tau_{\mathrm{exc}}^{\mathrm{blend}} = \frac{\tau_{\mathrm{exc}}^{\mathrm{polymer}}}{1 + A\tau_{\mathrm{exc}}^{\mathrm{polymer}} c_{\mathrm{fullerene}}} \quad (1)$$

where $\tau_{\mathrm{exc}}^{\mathrm{blend}}$ is the polymer emission lifetime when blended with fullerenes, $\tau_{\mathrm{exc}}^{\mathrm{polymer}}$ is the polymer emission lifetime of the neat RRa-P3HT, A is a fitting parameter that takes into account the quenching ability of the fullerene, and therefore varies between PCBM and bis-PCBM as can be seen in Figure 1d, and $c_{\mathrm{fullerene}}$ is the concentration of fullerene in the blend. The observed difference in quenching ability of the fullerenes could, in principle be attributed to the different electron affinities of the fullerenes and hence different driving forces for electron transfer. However, the nominal LUMO difference between RRa-P3HT and both PCBM and bis-PCBM far exceeds the 0.3–0.5 eV threshold needed for efficient charge generation. Some differences in quenching ability could however arise from variations in charge transfer rate due to variations in the donor-acceptor interface distances[23] and from disorder in the bis-PCBM acceptor strength.[24] The fitted curves are plotted in Figure 3 for the whole range of concentrations that has been studied experimentally in order to compare the experimental data with the model for dilute solid solution.

The polymer emission lifetime upon addition of fullerenes follows the dilute solid solution model up to about 25 vol% and 15 vol% for PCBM and bis-PCBM respectively. The saturation of the ultra-fast polymer emission for higher fullerene content has been previously reported by Bruno et al.[22,25] and has been assigned to aggregation of the blend components. Therefore, we tentatively assign the onset of aggregation of RRa-P3HT:PCBM and RRa-P3HT:bis-PCBM blends at 25 vol% and 15 vol% respectively.

As a consequence, we might expect to see evidence of a coarser microstructure in the RRa-P3HT:bis-PCBM sample than in a RRa-P3HT:PCBM sample at the same fullerene loading. In order to investigate this, we have conducted Transmission Electron Microscopy. Interestingly, no significant difference in microstructure is observed by TEM within the resolution of our measurement at 40–50 vol% of fullerene (see **Figure 4**) and both PCBM and bis-PCBM seem to be similarly well mixed.

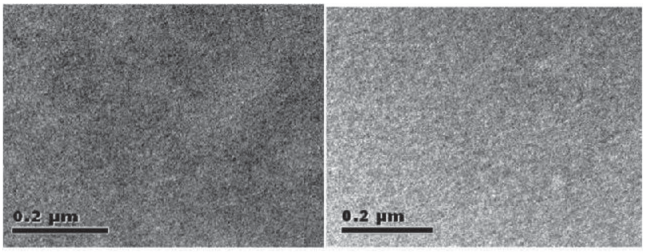

Figure 4. TEM images of a) RRa-P3HT:PCBM (43 vol%) and b) RRa-P3HT:bis-PCBM (52 vol%).

To summarize, ultra-fast PL spectroscopy points towards an onset of aggregation as low as 25 vol% and 15 vol% for PCBM and bis-PCBM respectively. Steady-state PL and UV–Vis absorption spectroscopy indicate that the backbones of RRa-P3HT are disturbed by the addition of up to about 25 vol% for both fullerene derivatives. Furthermore, no rougher phase separation is observed by TEM in the case of bis-PCBM. Note a very different behavior has been observed for PCBM and bis-PCBM blended with regioregular P3HT.[26]

2.2. Crystallinity of Fullerenes in RRa-P3HT

Demixing can be promoted by crystallization of one or both blend components, however, other mechanisms can lead to fullerene and polymer aggregation. Since crystallization may be beneficial for the charge separation process and the charge transport, it should be distinguished from aggregation. Therefore, we performed DSC on bulk samples of the two blend systems. We expect only PCBM to crystallize as a result of isomeric disorder of bis-PCBM.

DSC measurements for different PCBM content are plotted in **Figure 5**. All the structure in the traces is attributed to the melting of PCBM since RRa-P3HT is amorphous and, accordingly, no melting endotherms are observed in the neat RRa-P3HT DSC scan. Melting endotherms revealing the presence of crystallites of PCBM can be detected at content as low as 30 vol% of PCBM. This value therefore provides an upper limit for the onset of PCBM crystallization. Some crystallites may form for lower content but are not detectable by DSC. As expected, no melting endotherm due to the presence of crystallites is observed for bis-PCBM by DSC, which agrees with the lack of crystallization capability for this system according to X-ray diffraction experiments.[27] The DSC study thus confirms the presence of fullerene crystallites only in the case of PCBM. Furthermore, note that as in our previous work,[26,28] we observe a noticeable depression of the fullerene melting point upon addition of the polymer due to the partial miscibility of the two components.

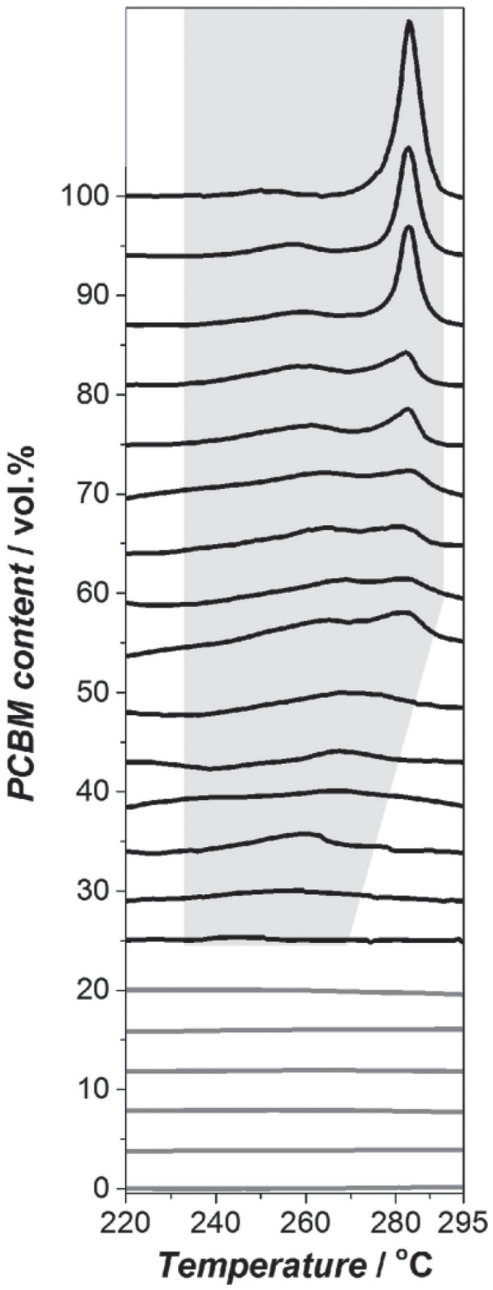

Figure 5. DSC scans of RRa-P3HT:PCBM blends of different fullerene loading at a heating rate of 20 °C/min.

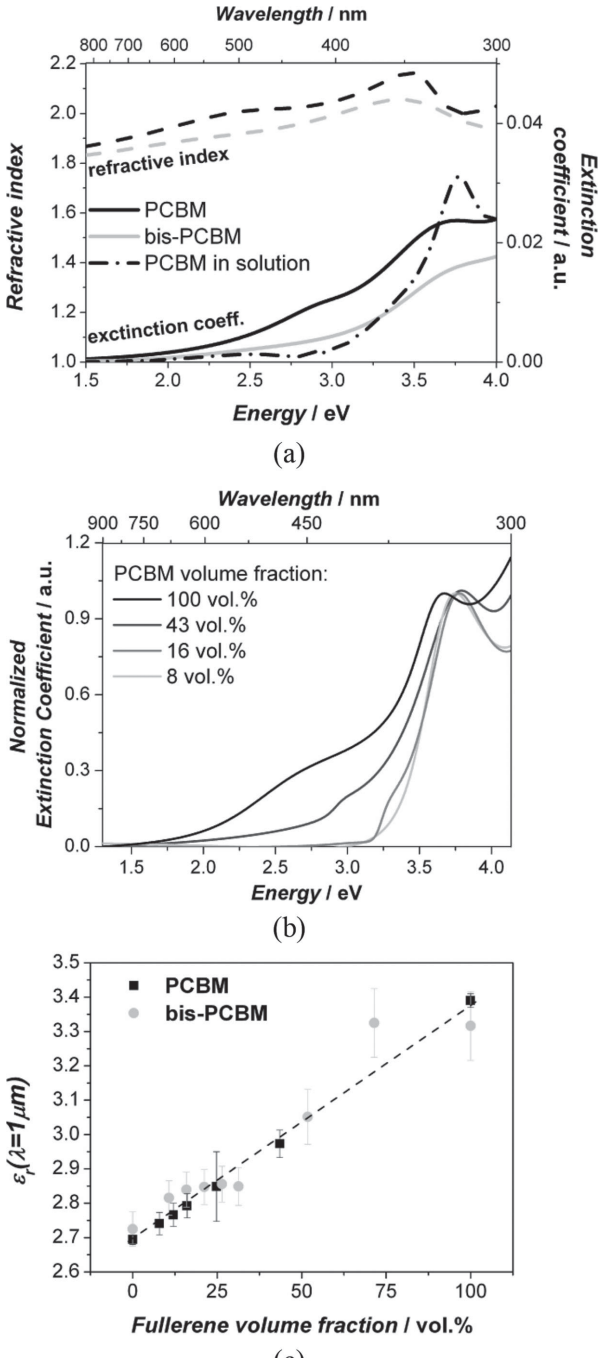

Figure 6. a) Refractive index and extinction coefficient of neat PCBM and bis-PCBM thin films extracted from VASE. The extinction coefficient of PCBM in solution measured by UV–Vis absorption spectroscopy is added for reference. b) PCBM extinction coefficients extracted from VASE of PCBM blended with RRa-P3HT for different PCBM loading. c) Optical dielectric constant ε_r extracted from the refractive index at 1 μm (≈1.24 eV) (the refractive index of blends extracted from VASE can be found in Supporting Information).

In order to study the state of the fullerene in thin films that are comparable with the photoactive layer in devices, we used VASE as a complementary, optical probe of microstructure. The refractive index and extinction coefficient of PCBM and bis-PCBM thin films extracted from VASE are plotted in **Figure 6**a. A larger refractive index is observed for PCBM indicating a denser packing of fullerenes in PCBM than in bis-PCBM. This can arise from either the extra side chains of bis-PCBM requiring more free volume or from crystallisation leading to dense packing only in the case of PCBM. Both PCBM and bis-PCBM extinction spectra exhibit a feature centered at ≈3.6 eV (≈345 nm). The PCBM extinction coefficient spectrum features an additional shoulder at low energies, which is not present in the bis-PCBM spectrum. This shoulder disappears for absorption spectra of PCBM in

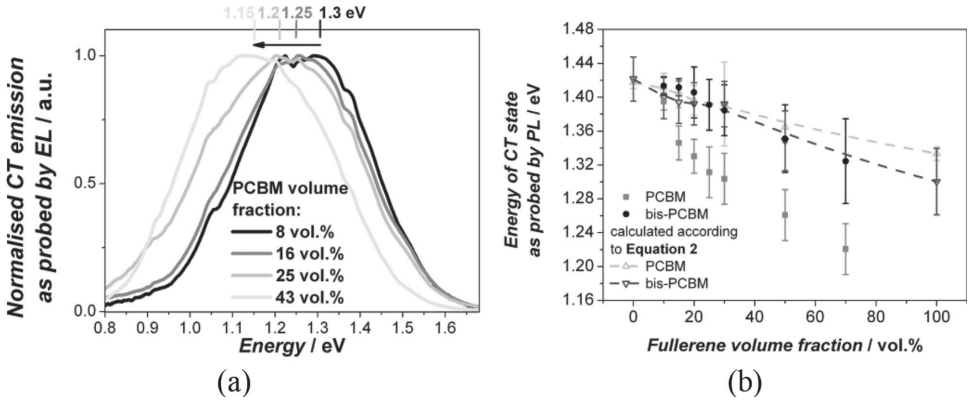

Figure 7. a) Normalized electroluminescence spectra of RRa-P3HT:PCBM blends. b) Energy of the CT peak extracted from the steady-state PL spectra as a function of the fullerene volume fraction. The steady-state PL spectra are plotted in the Supporting Information. The samples were excited with a laser at 473 nm.

solution, therefore is attributed to molecular packing in the solid state.

In order to quantify the composition dependence of this low energy shoulder we analyze the experimental VASE data as follows. For each composition we assume that the optical data refer to a blend of RRa-P3HT and a second material, combined using the Bruggeman approximation. The optical properties of the second material required to fit the experimental data are then extracted. These synthetic optical data are assigned to the fullerene in situ within the blend, and vary with composition. Note that the polymer optical properties are thought not to change significantly with mixing. The composition dependent extinction coefficient of PCBM extracted in this way is plotted in Figure 6b. For all blends, the high energy peak remains unshifted around the energy found for dilute solution of fullerenes. In the case of PCBM a low energy shoulder appears at fullerene content higher than about 15 vol%, which broadens and shifts towards lower energies with increasing fullerene content. In the case of bis-PCBM the extinction coefficient remains similar to the spectrum of PCBM in solution over the full range of studied concentrations.

We now estimate the effective optical dielectric constant ε_r of the blends of RRa-P3HT:PCBM and RRa-P3HT:bis-PCBM in order to evaluate the influence of varying dielectric constants on the CT emission. For this, we consider the film as an alloy, composed of an effective material with given optical properties that we deduce using the Cauchy and the standard critical point models.[29,30] The refractive indices for the two systems as a function of composition, as well as the deduced film thicknesses are given in Figure S5,S6 in Supporting Information, respectively. The optical dielectric constant, approximated by the square of the refractive index at 1 μm wavelength (i.e., in the transparency), is plotted as a function of the fullerene content in Figure 6c for both RRa-P3HT:PCBM and bis-PCBM blends. The experimental optical dielectric constant increases with fullerene content in a similar way for PCBM and bis-PCBM, as one might expect from an effective medium approximation.

We now address the origin of the low energy shoulder in PCBM blend films. The shift to lower energies of this shoulder could, in principle, be attributed to either a change in dielectric constant of the material[8] or to lowering of the fullerene excited state energy levels as a result of fullerene crystallization[31] leading to greater delocalization of the electron wavefunctions.[32]

Electroluminescence (EL) spectroscopy of charge transfer state emission is an in-situ probe of the energy difference between acceptor LUMO and donor HOMO,[33–36] and has previously been used to track changes in this energy difference in blend films of varying fullerene content.[37] Thus, studying the CT emission energy should indicate possible fullerene LUMO stabilization. The electroluminescence spectra for RRa-P3HT:PCBM blends are plotted in **Figure 7**a. Since it was not possible to measure EL spectra for RRa-P3HT:bis-PCBM because of poor performances of those materials in devices, CT state emission was also measured in both RRa-P3HT:PCBM and RRa-P3HT:bis-PCBM blends by means of photoluminescence detecting with an InGaAs photodiode array to probe energies down to 0.8 eV. PL has been previously used to track the CT emission energy as a function of blend composition.[38] The spectra can be found in Figure S7 in the Supporting Information. The energy of the CT peak determined by PL is plotted as a function of the fullerene volume fraction for RRa-P3HT:PCBM and bis-PCBM in Figure 7b.

A clear red-shift of the CT energy is observed when increasing the fullerene content for both PCBM and bis-PCBM.[39] However, the red-shift of the CT energy is much more pronounced in the case of PCBM.[40] Since a similar trend is observed for RRa-P3HT:PCBM for both electroluminescence and photoluminescence (the energy of CT peak determined by EL is plotted as a function of the fullerene volume fraction in Figure S8 in Supporting Information), the observed trend by photoluminescence is likely to be related to states that are involved in photocurrent generation, rather than emission from defect states, for example. The red shift of the CT state can be explained by a change in dielectric constant of the material or/and by a reduction of the energy levels as a result of greater delocalization of the electron wavefunctions. However, we showed earlier that the change in optical dielectric constant upon addition of PCBM and bis-PCBM is similar. Thus, the more pronounced red-shift in the case of PCBM cannot be solely explained by the change of dielectric constant, as previously shown by Bernado

et al.[36] We have plotted in Figure 7b the calculated energy of the CT state using the following equation:[8]

$$E_{CT} = E_0 - Z\left(1 - \frac{1}{\langle \varepsilon_r \rangle}\right)\left(\frac{1}{r^+} + \frac{1}{r^-}\right) - \frac{Z}{\langle \varepsilon_r \rangle}\left(\frac{2}{R_{CC}}\right) \quad (2)$$

where E_{CT} is the energy of the CT state, E_0 is a system dependent energy (here E_0 = 1.06 eV), $Z = \frac{e^2}{8\pi\varepsilon_0}$ (e being the electron charge, ε_0 the vacuum permittivity), $<\varepsilon_r>$ is the average relative permittivity (we use the optical dielectric constant extracted from VASE, see Figure 6c), r^+ and r^- are the effective radii of RRa-P3HT radical cation and the fullerene radical anion respectively (we took r^+ = 4.5 Å and r^- = 5.6 Å for both PCBM and bis-PCBM as in the paper from Veldman et al.[8] and R_{CC} is the centre-to-centre distance of mass (we choose R_{CC} = 11 Å to fit the bis-PCBM data and use the same value for PCBM). Note that any reasonable variations (<33%) of r^- and R_{CC} between PCBM and bis-PCBM lead to small variations in the CT state energy (<%) and thus, cannot explain the difference in energy of the CT state as observed by PL. The calculated energy of CT state is similar for both PCBM and bis-PCBM and follows the trend of the energy of CT state of RRa-P3HT:bis-PCBM as measured by photoluminescence. Thus, the red-shift of the energy of the CT state in the case of bis-PCBM can be explained solely by the variation of dielectric constant. However, the further red-shift in the case of PCBM cannot be explained by a dielectric effect and is tentatively assigned to the lowering of the energy levels of the crystallites as a result of greater delocalization of the electron wavefunctions.

3. Discussion and Conclusion

To summarize, we have demonstrated that we can probe the degree of mixing of fullerenes in an amorphous polymer matrix and, interestingly, distinguish between crystalline and amorphous fullerene clusters using a combination of spectroscopy methods: UV–Vis absorption, steady-state and ultrafast photoluminescence, VASE and electroluminescence. The values found for the degree of mixing, aggregation and crystallinity limits deduced using this combination of spectroscopic methods is summarized in **Table 1**.

Steady-state PL and UV–Vis absorption spectroscopies indicate good mixing of RRa-P3HT with both fullerenes up to 25 vol% fullerenes. Ultra-fast PL spectroscopy points towards an onset of aggregation as low as 25 vol% and 15 vol% for PCBM and bis-PCBM respectively.

DSC gives evidence of the presence of PCBM crystallites down to 30 vol% only in the case of PCBM. Our analysis using VASE shows that for both PCBM and bis-PCBM, the dielectric constant increases upon addition of fullerene but only PCBM shows features (appearance of a low energy shoulder) in the extinction coefficient spectra. Those features are detected for volume fractions as low as about 15 vol%. This low energy shoulder shifts to lower energies as the PCBM content increases. Using electroluminescence and photoluminescence, we showed that this shift can be attributed to the delocalization of the electron wavefunctions as a result of PCBM crystallization.

In fact, we observed that although the change of dielectric constant as extracted by VASE is similar upon addition of PCBM and bis-PCBM, the energy of the CT state is further red-shifted in the case of PCBM. Thus, we conclude that the red-shift of the CT state energy is due to the change in dielectric constant for bis-PCBM and to both change in dielectric constant and delocalization of the wavefunction across the fullerene crystallites for PCBM.

We further conclude that the difference in behavior of the photoluminescence decay time between PCBM and bis-PCBM at concentrations higher than the onset of aggregation and the shift of the low energy shoulder observed on the PCBM extinction coefficient spectra extracted by VASE are both due to crystallization of PCBM while bis-PCBM clusters remain amorphous. We speculate that the delocalization of the electron wavefunction across the PCBM crystallites enhances the charge separation rate and thus, reduces geminate recombination, leading to a shorter polymer photoluminescence decay time. Moreover, the delocalization of the electron wavefunction leads to further stabilization of the fullerene LUMO, and thus to a red-shift of the extinction coefficient edge.

Finally, as emphasized in the introduction, fullerene crystallization is of importance for charge separation and charge transport, and thus for OPV device performance in general. Even if a fullerene derivative is known to potentially crystallize, its ability to crystallize in a polymer matrix strongly depends on the polymer and the processing conditions (solvent, temperature, type of substrate, deposition technique and parameters etc.). Therefore, we propose that spectroscopic techniques such as electroluminescence, photoluminescence and VASE that allow for distinguishing between amorphous and crystalline

Table 1. Summary of the deduced values for the degree of mixing, aggregation and crystallinity limits using the different spectroscopic techniques.

		PCBM		bis-PCBM	
	Experiment	vol%	Variation	vol%	Variation
Mixing	RRa-P3HT blue shift	<25	60 meV	<25	60 meV
	RRa-P3HT absorption edge shift	<25	60 meV	<25	60 meV
Aggregation	Ultra-fast photoluminescence	>25	N.A.	>15	N.A.
Crystalline vs. amorphous fullerene clusters	VASE	>15	Appearance of low energy shoulder	N.A.	No features
	CT PL energy shift vs VASE ε_r	N.A.	20 meV	N.A.	10 meV

fullerene clusters may be of great interest for polymer:fullerene thin film characterization, especially because they could be in theory combined with AFM to spatially resolve the morphology of blends. Furthermore, being able to distinguish between crystalline and amorphous fullerene clusters will also allow direct correlation between fullerene crystallization and charge separation and transport properties, and more generally with OPV device performances. The methods used in this paper could be in principle extended to other polymers, especially high efficiency amorphous or weakly-crystalline low-bandgap polymers where the overlap between the emissions of the acceptor and the CT state is low. In the case of more crystalline polymers, the analysis of the PL quenching can be complicated by additional composition dependent non-radiative quenching and the appearance of a fast PL phase in the PL kinetics. The degree of crystallinity of the polymer as a function of the fullerene content may impact the CT energy, but this difficulty can be overcome by studying the polymer with both an amorphous and a semi-crystalline fullerene.

4. Experimental Section

Materials and Solutions: PCBM and bis-PCBM were supplied by Solenne BV with molecular weights of 910.88 and 1101.10 g/mol, respectively. The purity of both PCBM and bis-PCBM is superior to 99.5%. RRa-P3HT was purchased from Sigma-Aldrich (Rieke Metals, Mw = 100 K, PDI = 3 as determined by gel permeation chromatography—see Figure S9 in Supporting Information, RR = 53% and purity superior to 90% as determined by nuclear magnetic resonance—see Figure S10 in Supporting Information). All chemicals were used as received. Thin films for spectroscopy were fabricated by spin-coating of material mixtures (10 mg mL^{-1}) from chlorobenzene onto quartz substrates. Bulk heterojunction (BHJ) solar cells were prepared by cleaning patterned ITO in detergent, acetone, and isopropanol in ultrasonic bath. The ITO substrates were further treated with oxygen plasma for 5 min. A 30 nm-thick layer of PEDOT:PSS was blade coated onto the ITO substrates and annealed at 150 °C for 20 min. Subsequently, the active layer solution was blade coated on top from a solution of RRa-P3HT polymer and fullerene dissolved in a chloroform/o-dichlorobenzene (4:1) mixed solvent. These optimum conditions for processing the films via blade coating were determined by a series of experiments to keep the film thickness in the range of 100–120 nm. The polymer and fullerene are mixed at different weight percentages, from pure polymer to pure fullerene (25 mg mL^{-1}). The organic active layers were coated in air and transferred to a nitrogen filled glove box (<0.1 O_2, H_2O), where calcium/aluminium (20 nm/150 nm) were vacuum-deposited as cathode. The thin films for low energy PL measurement were blade coated in the air on microscope glass slides which had previously been cleaned with detergent, acetone, and isopropanol.

Absorption and Photoluminescence: Steady-state UV–Vis absorption data on thin films were measured using a Perkin-Elmer Lambda 25 spectrophotometer. Steady-state UV–Vis absorption data on solutions were measured using a homemade set up. Steady-state PL was collected using two pieces of equipment: a Horiba Jobin Yvon Fluorolog-2 PL spectrometer, and a LabRamHR800 spectrometer. Moreover, steady-state photoluminescence at low energies was measured with the same detector and monochromator system as electroluminescence (see below). An additional 595 nm long pass filter was used to filter out the laser wavelength.

Fitting Protocol for Polymer PL Spectra: The PL spectra of the pure polymers were fitted using up to five equidistant Gaussian functions to represent the Franck-Condon series corresponding to optical transitions between the vibrational ground state of the LUMO and the ground and excited vibrational states of the HOMO (0–0 to 0–4 transitions). All Gaussian peaks have the same width and a spacing of 175 meV, corresponding to the average vibrational frequency characteristic of the HOMO energy levels. For the blends, it was assumed that the form of the polymer emission remains unchanged. This means that the ratios of the peak integrated intensities (amplitude multiplied by the width) and the peak spacing were kept fixed, as if the Huang-Rhys factor is not affected by blending. The fact that the lineshape fitting performed well in the high energy region of the 0–0 and 0–1 transitions provides support to the previous assumption. Hence, for the fits the polymer PL spectrum as a whole was allowed to shift in energy and rigidly change in intensity upon blending. A slight change in the width of the peaks was also allowed. Furthermore, the PCBM and bis-PCBM PL contribution was taken into account by modeling the emission in films of the pure components. Finally, an additional Gaussian peak at low energies took care of the contribution stemming from radiative recombination of charge-transfer excitons.

Ultrafast Time-resolved Photoluminescence: Ultrafast time-resolved photoluminescence decays were measured using the femtosecond up-conversion technique. The samples were held in a nitrogen atmosphere and continuously translated through the excitation beam to eliminate photobleaching effects and local degradation of the films. Excitation was below the onset of intensity-dependent kinetics and was performed with the frequency-doubled (400 nm) output of a mode locked Ti:sapphire laser supplying 70 fs pulses at 800 nm with a repetition rate of 80 MHz. The emission at 620 nm was upconverted in a beta-barium-borate crystal using the fundamental laser beam at 800 nm as the gate. Sum-frequency photons were dispersed in a monochromator and detected using a photomultiplier tube. The temporal resolution of the system was ≈150 fs.

Transmission Electron Microscopy: For TEM images, the P3HT:fullerene films were floated onto the surface of deionized water and caught on 300 mesh copper grids. TEM images were obtained using a JEOL 2000FX electron microscope operated at 200 kV.

Differential Scanning Calorimetry: Thin films were drop-cast from the homogeneous solutions onto glass slides, followed by evaporation of the solvent at room temperature. Afterward, the thin films were scratched, and the "powder" was placed in aluminium pans to be analyzed. The sample weight was about 5 mg. DSC was conducted under nitrogen at three different heating rates: 2, 10, and 20 °C min^{-1} and a cooling rate of 10 °C min^{-1} with a Metler Toledo DSC822 instrument.

Variable Angle Spectroscopic Ellipsometry: Variable angle spectroscopic ellipsometry (VASE) measurements were carried out using a SOPRALAB GES5E rotating polarizer ellipsometer installed within a clean room that uses a Xe lamp as a light source and a CCD detector to record optical spectra from ca. 1.2 eV to 5.6 eV. Three incidence angles were typically recorded for each sample, varying between 55 and 75 degrees. The refractive indices for the pure materials were deduced from the corresponding VASE data using the standard critical point model.[30] The data for the blends were analyzed in two different ways, either as mixtures of the polymer and effective fullerene with an unknown optical property, or as an alloy with effective optical properties for the whole blend.

Electroluminescence: Electroluminescence (EL) was measured at various forward injection current densities. Emission was detected using a Princeton Instruments Acton SP 2500 monochromator combined with a liquid nitrogen cooled InGaAs Photodiode array (Acton OMAV: 1024), while the injection current was controlled with a Keithley 3801 sourcemeter. The spectral sensitivity was corrected with the spectrum from a calibrated halogen lamp.

Supporting Information

Supporting Information is available from the Wiley Online Library or from the author.

Acknowledgements

The authors would like to acknowledge Dr. Raja Shahid Ashraf (Department of Chemistry, Imperial College London) for GPC and NMR. This work was supported by EPRSC (EP/G031088 and EP/K030671) and the SUPERGEN Excitonic Solar Cell Consortium. We are grateful to the Ministerio de Economía y Competitividad for funding through projects CSD2010–00044 (Consolider NANOTHERM), MAT2009–10642 and MAT2012–37776. A.A.Y.G. acknowledges the EPSRC for award of a Doctoral Prize Fellowship. M.S. acknowledges a JAE-PRE grant from CSIC which is co-financed by the European Social Fund. A.B. wishes to acknowledge MIUR Public-PrivateLaboratory Project PO2_00556_33069378 RELIGHT) for partial financial support. J.Y. acknowledges funding via the Imperial College Rector's Scholarship. T.K. acknowledges funding via an Imperial College Junior Research Fellowship. J.N. acknowledges the award of an Industry Fellowship from the Royal Society.

Received: May 19, 2014
Revised: July 13, 2014
Published online: September 2, 2014

[1] C. J. Brabec, S. Gowrisanker, J. J. M. Halls, D. Laird, S. Jia, S. P. Williams, *Adv. Mater.* **2010**, *22*, 3839.
[2] W. Yin, M. Dadmun, *ACS Nano* **2011**, *5*, 4756.
[3] N. Treat, M. A. Brady, G. Smith, M. F. Toney, E. J. Kramer, C. J. Hawker, M. L. Chabinyc, *Adv. Energy Mater.* **2011**, *1*, 82.
[4] K. H. Lee, Y. Zhang, P. L. Burn, I. R. Gentle, M. James, A. Nelson, P. Meredith, *J. Mater. Chem. C* **2013**, *1*, 2593.
[5] B. A. Collins, E. Gann, L. Guignard, X. He, C. R. McNeill, H. Ade, *J. Phys. Chem. Lett.* **2010**, *1*, 3160.
[6] R. C. Nieuwendaal, C. R. Snyder, R. J. Kline, E. K. Lin, D. L. VanderHart, D. M. DeLongchamp, *Chem. Mater.* **2010**, *22*, 2930.
[7] N. D. Treat, A. Varotto, C. J. Takacs, N. Batara, M. Al-Hashimi, M. J. Heeney, A. J. Heeger, F. Wudl, C. J. Hawker, M. L. Chabinyc, *J. Am. Chem. Soc.* **2012**, *134*, 15869.
[8] D. Veldman, O. Izpek, S. C. J. Meskers, J. Sweelsen, M. M. Koetse, S. C. Veenstra, J. M. Kroon, S. S. van Bavel, J. Loos, R. A. J. Janssen, *J. Am. Chem. Soc.* **2008**, *130*, 7721.
[9] F. C. Jamieson, E. Buchaca Domingo, T. McCarthy-Ward, M. Heeney, N. Stingelin, J. R. Durrant, *Chem. Sci.* **2012**, *3*, 485.
[10] B. M. Savoie, A. Rao, A. A. Bakulin, S. Gelinas, B. Movaghar, R. H. Friend, T. J. Marks, M. A. Ratner, *J. Am. Chem. Soc.* **2014**, *136*, 2876.
[11] H. Hoppe, M. Niggemann, C. Winder, J. Kraut, R. Hiesgen, A. Hinsch, D. Meissner, N. S. Sariciftci, *Adv. Funct. Mater.* **2004**, *14*, 1005.
[12] U. Zhokhavets, T. Erb, G. Gobsch, M. Al-Ibrahim, O. Ambacher, *Chem. Phys. Let.* **2006**, *418*, 347.
[13] M. Hallermann, I. Kriegel, E. Da Como, J. M. Berger, E. von Hauff, J. Feldmann, *Adv. Func. Mater.* **2009**, *19*, 3662.
[14] Z. Mao, K. Vakhshouri, C. Jaye, D. A. Fischer, R. Fernando, D. M. DeLongchamp, E. D. Gomez, G. Sauve, *Macromolecules* **2013**, *46*, 103.
[15] D. Jarzab, F. Cordella, M. Lenes, F. B. Kooistra, P. W. M. Blom, J. C. Hummelen, M. A. Loi, *J. Phys. Chem. B* **2009**, *113*, 16513.
[16] D. E. Motaung, G. F. Malgas, C. J. Arendsen, *Synth. Met.* **2010**, *160*, 876.
[17] P. Westacott, J. R. Tumbleston, S. Shoai, S. Fearn, J. Bannock, J. Gilchrist, S. Heutz, J. de Mello, M. Heeney, H. Ade, J. Durrant, D. McPhail, N. Stingelin, *Energy Environ. Sci.* **2013**, *6*, 2756.
[18] C. Müller, J. Bergqvist, K. Vandewal, K. Tvingstedt, A. S. Anselmo, R. Magnusson, M. I. Alonso, E. Moons, H. Arwin, M. Campoy-Quiles, O. Inganäs, *J. Mater. Chem.* **2011**, *21*, 10676.
[19] A. Petrozza, F. Laquai, I. A. Howard, J.-S. Kim, R. H. Friend, *Phys. Rev. B* **2010**, *81*, 205421.
[20] P. Parkinson, C. Müller, N. Stingelin, M. B. Johnston, L. M. Herz, *J. Phys. Chem. Lett.* **2010**, *1*, 2788.
[21] S. D. Stranks, C. Weisspfennig, P. Parkinson, M. B. Johnston, L. M. Herz, R. J. Nicholas, *Nano Lett.* **2011**, *11*, 66.
[22] A. Bruno, L. X. Reynolds, C. Dyer-Smith, J. Nelson, S. A. Haque, *J. Phys. Chem. C.* **2013**, *117*, 19832.
[23] E. Busby, C. W. Rochester, A. J. Moule, D. S. Larsen, *Chem. Phys. Lett.* **2011**, *513*, 77.
[24] J. M. Frost, M. A. Faist, J. Nelson, *Adv. Mater.* **2010**, *22*, 4881.
[25] O. V. Mikhnenko, H. Azimi, M. Scharber, M. Morana, P. W. M. Blom, M. A. Loi, *Energy Environ. Sci.* **2012**, *5*, 6960.
[26] A. A. Y. Guilbert, L. X. Reynolds, A. Bruno, A. MacLachlan, S. P. King, M. A. Faist, E. Pires, J. E. Macdonald, N. Stingelin, S. A. Haque, J. Nelson, *ACS Nano*, **2012**, *6*, 3868.
[27] M. H. Yun, G.-H. Kim, C. Yang, J. Y. Kim, *J. Mater. Chem.* **2010**, *20*, 7710.
[28] C. Müller, T. A. M. Ferenczi, M. Campoy-Quiles, J. M. Frost, D. D. C. Bradley, P. Smith, N. Stingelin-Stutzmann, J. Nelson, *Adv. Mater.* **2008**, *20*, 3510–3515.
[29] M. Campoy-Quiles, J. Nelson, D. D. C. Bradley, *Phys. Rev. B* **2007**, *76*, 235206.
[30] M. Campoy-Quiles, M. I. Alonso, D. D. C. Bradley, L. J. Richter, *Adv. Funct. Mater.* **2014**, *24*, 2116.
[31] K. Vandewal, W. D. Oosterbaan, S. Bertho, V. Vrindts, A. Gadisa, L. Lutsen, D. Vanderzande, J. V. Manca, *Appl. Phys. Lett.* **2009**, *9*, 123303.
[32] K. R. Graham, P. Erwin, D. Nordlund, K. Vandewal, R. Li, G. O. Ngongang Ndjawa, E. T. Hoke, A. Salleo, M. E. Thompson, M. D. McGehee, A. Amassian, *Adv. Mater.* **2013**, *25*, 6076.
[33] P. Panda, D. Veldman, J. Sweelssen, J. J. A. M. Bastiaansen, B. M. W. Langeveld-Voss, S. C. J. Meskers, *J. Phys. Chem. B* **2007**, *111*, 5076.
[34] K. Tvingstedt, K. Vandewal, A. Gadisa, F. Zhang, J. Manca, O. Inganas, *J. Am. Chem. Soc.* **2009**, *131*, 11819.
[35] M. A. Faist, T. Kirchartz, W. Gong, R. S. Ashraf, I. McCulloch, J. C. de Mello, N. J. Ekins-Daukes, D. D. C. Bradley, J. Nelson, *J. Am. Chem. Soc.* **2012**, *134*, 685.
[36] B. Bernardo, D. Cheyns, B. Verreet, R. D. Schaller, B. P. Rand, N. C. Giebink, *Nat. Comm.* **2014**, *5*, 3245.
[37] S. A. Hawks, F. Deledalle, J. Yao, D. G. Rebois, G. Li, J. Nelson, Y. Yang, T. Kirchartz, J. R. Durrant, *Adv. Energy Mater.* **2013**, *3*, 1201.
[38] M. A. Loi, S. Toffanin, M. Muccini, M. Forster, U. Scherf, M. Scharber, *Adv. Funct. Mater.* **2007**, *17*, 2111.
[39] M. L. Tietze, W. Tress, S. Pfützner, C. Schünemann, L. Burtone, M. Riede, K. Leo, K. Vandewal, S. Olthof, P. Schulz, A. Kahn, *Phys. Rev. B* **2013**, *88*, 085119.
[40] F. Piersimoni, S. Chambon, K. Vandewal, R. Mens, T. Boonen, A. Gadisa, M. Izquierdo, S. Filippone, B. Ruttens, J. D'Haen, N. Martin, L. Lutsen, D. Vanderzande, P. Adriaensens, J. V. Manca, *J. Phys. Chem. C* **2011**, *115*, 10873.